Advances in plasma-based beam dump modelling

Journal of Physics: Conference Series **1596** (2020) 012058 doi:10.1088/1742-6596/1596/1/012058

Advances in plasma-based beam dump modelling

A Bonatto[1,2], R P Nunes[3], O Jakobsson[1], B Williamson[1,2], L Liang[1,2], and G Xia[1,2]

[1]School of Physics and Astronomy, University of Manchester, Oxford Road, Manchester M13 9PL, United Kingdom
[2]The Cockcroft Institute, Sci-Tech Daresbury, Daresbury, Warrington, WA4 4AD, United Kingdom
[3]Departamento de Engenharia Elétrica, Escola de Engenharia, Universidade Federal do Rio Grande do Sul, Porto Alegre, Brazil

E-mail: alexandre.bonatto@manchester.ac.uk

E-mail: guoxing.xia@manchester.ac.uk

Abstract. This work presents a short review on the advances of plasma beam dump modelling since they have been first proposed. Analytical models have been derived to estimate the beam energy loss for both passive and active beam dump schemes. For the passive case in particular, tailored plasma density profiles can improve beam-energy extraction by mitigating particle re-acceleration. A semi-analytical model, consisting of the dynamics of test-particles experiencing the previously derived analytical wakefields, is under development to investigate deceleration beyond the saturation point, in the linear to the quasi-linear regime.

1. Introduction

Under proper conditions, laser pulses or particle beams can excite intense wakefields when propagating in plasmas [1]. In plasma-based accelerators [2, 3, 4], wakefields with accelerating gradients of ∼GV/cm [3] can produce high-quality, multi-GeV beams over a few centimetres of propagation distance [4]. These gradients are orders of magnitude higher than those obtained with conventional accelerator techniques (∼MV/m). Although this technology has potential to enable the design of compact, transportable applications [5], their overall compactness may be limited by large and heavy beam dumps required for the safe disposal of high-energy beams. An alternative to overcome this limitation is the implementation of plasma beam dumps.

Plasma-based beam dumps make use of the decelerating phase of the wakefields to achieve compact deceleration of spent beams. Long-range interactions from plasma collective behaviour may greatly enhance the beam-energy extraction if compared to the short-range, individual particles interactions [6]. Moreover, since deceleration in a low-density plasma medium produces much less radionuclides than in high-density solid targets used in conventional beam dumps, plasma-based dumps greatly reduce radiation hazards [6, 7]. In addition, the possibility of recovering the energy deposited into the plasma turns the adoption of plasma beam dumps an important milestone to develop safer and greener facilities.

The present work is organised as follows. In section 2, the passive plasma beam dump scheme, in which deceleration is achieved by the beam self-driven wakefield, is discussed. In section 3, the active plasma beam dump scheme, in which the beam is loaded in the decelerating phase of a

laser-driven wakefield, is described. Both sections are short reviews regarding the work that has been done and published in this field, as well as the main references in the subject. In section 4, tailored plasma-density profiles are discussed as an alternative to improve the beam-energy extraction in the passive beam dump scheme. This section describes theoretical advances recently proposed to overcome the energy loss saturation observed in the passive scheme when a uniform plasma-density profile is adopted. In section 5, a semi-analytical model is introduced. This model, based on test-particles experiencing the wakefields given by the existing analytical solutions, might be able to describe the beam particles dynamics in both passive and active plasma beam dump schemes. Although the semi-analytical model is still under development, the preliminary results here presented show the potential of this method. Finally, section 6 summarizes the main advantages and disadvantages of both passive and active plasma beam dump schemes. In addition, brief discussions regarding tailored plasma-density profiles, and the semi-analytical model currently under development are presented.

2. Passive plasma beam dump

In the passive beam dump, an electron beam propagating in an undisturbed plasma is decelerated by its self-driven wakefield. The longitudinal and transverse components of this wakefield have initial decelerating and focusing phases, respectively. Therefore, a beam shorter than $\lambda/2$, where λ is the plasma wavelength, will be simultaneously decelerated and focused as it propagates in the plasma. Chou *et al* . [8] observed experimental evidence of passive plasma-based deceleration, achieving an average decelerating gradient of 5.1 GV/m, with peak higher than 14 GV/m. In comparison to conventional collisional and radiative energy loss [9], as well as betatron radiation loss [10], these values exceed them by a factor of $> 10^4$.

In the passive scheme, analytical models for the evolution of the total beam-energy $U(s)/U_0$, where $U(s) = \sum_{i=1}^{N} E_{ki}(s)$, being N the number of beam particles, $E_{ki}(s)$ the kinetic energy of the ith particle at the propagation distance s, and $U_0 \equiv U(s=0)$ the total beam initial energy, are available for beams with parabolic transverse and half-sine [7] or Gaussian [11] longitudinal density profiles. These models, developed assuming a uniform plasma-density profile under a frozen-beam approximation, show that the beam total-energy loss is linear until one of the beam particles reaches $\gamma_i(s)/\gamma_{i0} \simeq 0$, where $\gamma_i(s)$ is the Lorentz relativistic factor for the ith particle at s, and $\gamma_{i0} \equiv \gamma_i(s=0)$. However, since the decelerating wakefield E_z rises from zero at the head of the beam to a maximum value $E_{z,max}$ at a certain position towards its tail, the energy extraction is chirped in this scheme; particles experiencing $E_{z,max}$ reach $\gamma_i/\gamma_{i0} \ll 1$ while particles at the head of the beam preserve most of their initial energy. Due to dephasing, decelerated particles reach the next accelerating phase of the wakefield, causing the formation of re-acceleration peaks that saturate the net beam-energy extraction. The saturation distance s^*, i.e., the distance at which particles under the maximum wakefield $E_{z,max}$ reach the condition $\gamma_i/\gamma_{i0} \ll 1$ and suffer phase slippage, is given by $s^* = \gamma_0/[k_p\, E_{z,max}/E_0]$, where $k_p = \omega_p/c$ is the plasma wave number, $\omega_p = (n_0 e^2/m_e\epsilon_0)^{1/2}$ is the plasma frequency, c is the speed of light in vacuum, ϵ_0 is the free space permittivity, e and m_e are the electron charge and mass, respectively, and $E_0 = cm_e\omega_p/e$ is the cold non-relativistic wave breaking electric field. The behaviour above described can be observed in Figure 1, which contains both analytical and numerical results for a beam undergoing a passive plasma beam dump. Numerical results were obtained from 2D axisymmetric simulations performed with the FBPIC code [12].

3. Active plasma beam dump

In the active beam dump, a preceding laser driver enhances the decelerating wakefield produced by the beam on the plasma. The resulting net wakefield along the beam is then the superposition of both laser and beam-driven wakefields. If proper parameters are chosen for the laser pulse

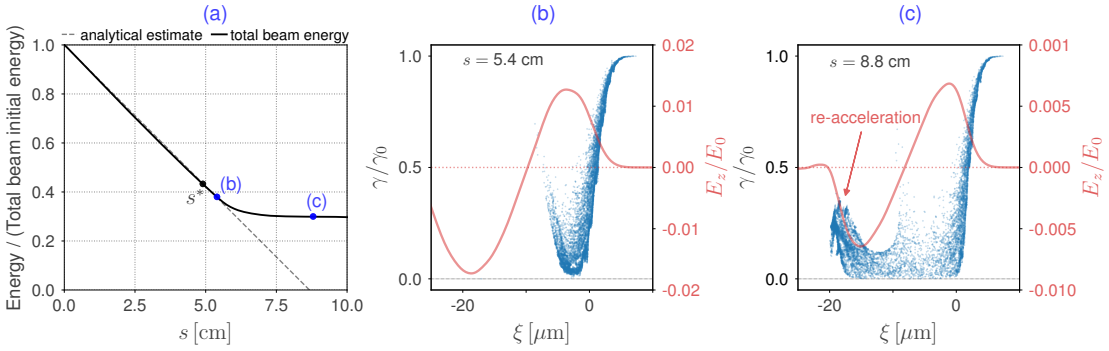

Figure 1. Passive plasma beam dump. A bi-Gaussian electron beam, initially monoenergetic ($E_{k0} = 1$ GeV), with charge $Q_b = 30$ pC, longitudinal and transverse RMS sizes of $\sigma_z = 2$ μm and $\sigma_r = 1.4$ μm, respectively, propagates in a uniform plasma with density $n_0 \simeq 10^{18}$ cm^{-3}. (a) Total beam-energy loss from the analytical model (*black, dashed line*) shows good agreement with PIC simulation results (*black, thick line*). After the saturation distance $s^* \simeq 5$ cm, (b) particles experiencing higher values of E_z (*red line*) reach $\gamma/\gamma_0 \ll 1$ ($\xi \equiv z - v_b t$ is the beam co-moving coordinate). (c) For $s \simeq 9$ cm, an appreciable quantity of beam particles form a re-acceleration peak. Panel (a) shows that the beam energy extraction saturates at $U/U_0 \simeq 0.3$.

and its phase with respect to the beam, it is possible to obtain a quasi-flat wakefield along the beam, with amplitude higher than that of both individual wakefields. As a consequence, the beam energy is extracted with a small, residual chirp, in a much shorter distance if compared to the passive case. An analytical model for the total energy loss of beams with transverse parabolic and half-sine longitudinal density profiles is available for the active scheme [7]. This model was derived assuming the quasi-matched propagation [3] of a laser pulse in a plasma with a longitudinal uniform and parabolic transverse density profile. More details regarding the active plasma beam dump can be obtained from Bonatto *et al* . [7].

4. Tailored plasma-density profiles

As discussed in section 2, the beam-energy extraction in passive beam dumps with uniform plasma-density profiles is typically limited to $U/U_0 = 0.3 \sim 0.4$, due to the formation of re-acceleration peaks. Wu *et al* . [6] proposed the use of vacuum regions and periodic thin foils, placed along the plasma in specific positions to eliminate re-acceleration peaks. However, experimental implementation of this idea might be challenging. Hanahoe *et al* . [13] explored the use of linearly or quadratically increasing plasma-density profiles to defocus particles from re-acceleration peaks before they recover highly relativistic energies. Then, instead of the vacuum regions and planar thin foils inside the plasma, a vessel-shaped foil wrapped around the plasma cell could be used to stop the ejected particles. Final energies of $U/U_0 \simeq 0.25$ were obtained in 2D Cartesian simulations performed with VSim PIC code [14] for these profiles. Jakobsson *et al* . [15] extended the investigation on the use of tailored plasma-density profiles to eliminate re-acceleration peaks, providing a clearer understanding on the role played by the rate of plasma wavelength change with respect to the propagation distance s, $\lambda' \equiv d\lambda/ds$, in the energy of ejected particles. By changing the plasma density n, it is possible to control the plasma wavelength $\lambda \propto 1/\sqrt{n}$, hence the location of the accelerating/decelerating (longitudinal), and focusing/defocusing (transverse) phases of the wakefield. Since λ' can be interpreted as the speed at which the defocusing wakefield phase moves if observed from the co-moving coordinate $\xi \equiv z - v_b t$, plasma density profiles tailored to have higher values of λ' provide earlier defocusing of re-acceleration peaks. As a consequence, particles will remain less time under re-acceleration,

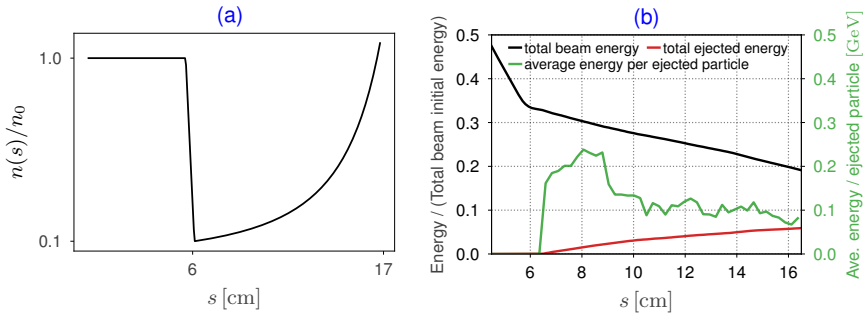

Figure 2. Passive beam dump with a tailored plasma-density profile. Beam parameters are $E_{k0} = 1$ GeV, $Q_b = 30$ pC, $\sigma_z = 2$ μm, and $\sigma_r = 1.4$ μm. Panel (a) shows a tailored-density profile, starting from $n_0 \simeq 10^{18}$ cm^{-3}. After the density drop, this profile provides a constant λ'. Panel 2(b) shows that a final beam-energy of $U/U_0 \simeq 0.2$ (*black, thick line*), and $\sim 6\%$ of the total beam initial energy was ejected (*red line*). After peaking at ~ 220 MeV, the average energy per ejected particle (*green line*) stabilizes around ~ 100 MeV.

being ejected at lower energies. Figure 2 shows an example of such tailored plasma-density profiles, as well as numerical results obtained from a 2D axisymmetric simulation performed with FBPIC for beam deceleration in a passive beam dump with such density profile. Beam parameters here are the same from Fig. 1. Figure 2(a) shows a tailored-density profile with ~ 6 cm of constant density $n_0 \simeq 10^{18}$ cm^{-3}, followed by a 10-fold density drop along a 5 mm-long linear down-ramp, and a specific density-increasing profile, providing a constant λ', which brings the density back to n_0 along ~ 10 cm of propagation. Figure 2(b) shows that a final beam-energy of $U/U_0 \simeq 0.2$ (*black, thick line*) was achieved, and $\sim 6\%$ of the total beam initial energy was transversely ejected (*red line*). After peaking at ~ 220 MeV, the average energy per ejected particle (*green line*) stabilizes around ~ 100 MeV. The adoption of an optimized density down-ramp profile [16, 17] might mitigate the observed peak in the average energy of the ejected particles. More details about tailored plasma-density profiles can be found in Jakobsson *et al* . [15].

5. Semi-analytical model

Analytical expressions are available for the wakefield excited in a uniform plasma by an electron beam with a longitudinal Gaussian and transverse parabolic density profile [7, 11, 18]. By using test-particles, a model can be derived to describe the particle-wave interaction associated with the decelerating process under discussion. In this approach, beam particles of mass m, and charge q are submitted to the action of the analytical wakefield $\mathbf{W} = E_z\,\hat{\mathbf{z}} + W_\perp \hat{\mathbf{r}}$, where $W_\perp = E_r - cB_\theta$ is the transverse wakefield in cylindrical coordinates. Since the fields (hence the forces) have cylindrical symmetry, the azimuthal dynamics of beam particles is neglected in this first attempt to implement the semi-analytical model. Under this assumption, the orbit of the test-particles $(\mathbf{r}, \mathbf{v})$ can be computed numerically by solving the relativistic Newton's second law $d(\gamma m\mathbf{v})/dt = q\mathbf{W}$, which assumes the following form,

$$\frac{d}{dt}(\gamma m v_z) = qE_z \quad , \quad \frac{d}{dt}(\gamma m v_r) = qW_\perp . \tag{1}$$

Since $\gamma = \gamma(v)$ and $v \simeq \sqrt{v_r^2 + v_z^2}$, the ordinary differential equations above form a coupled non-linear system. Figures 3(a) and 3(b) show a preliminary comparison between a PIC simulation, performed with FBPIC for a bi-Gaussian beam with the same parameters from section 4 ($E_{k0} = 1$

GeV, $Q_b = 30$ pC, $\sigma_z = 2$ μm, and $\sigma_r = 1.4$ μm) propagating in a uniform plasma of density $n_0 \simeq 10^{18}$ cm^{-3}, and the semi-analytical model. For that, a particle orbit is extracted from the PIC simulation and compared to the orbit obtained from the model, imposing the same initial conditions. The initial conditions of the particle under analysis are $r = 0.42$ μm, $v_r = 0$, $z = -2.65$ μm, and $v_z = v_b$, where v_b is the beam velocity, obtained from the initial beam energy.

Figure 3(a) shows how the radial coordinate r evolves with the propagation distance s. Despite the differences, there is a reasonable qualitative and quantitative agreement between the PIC simulation and the semi-analytical model results. The betatron oscillations of the simulations also exist in the model results, with similar period. Moreover, a peaked-like envelope modulation is shown in both cases, with similar amplitudes. The main difference observed is a shift in the peak location, which will be discussed further, since this behaviour is also observed in the other quantities to be compared. Figure 3(b) shows a similar behaviour for the evolution of the normalised radial velocity, v_r/c.

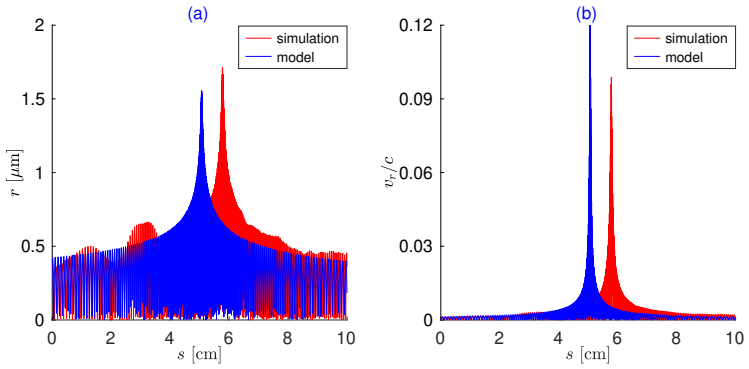

Figure 3. Transverse particle dynamics for (a) r and (b) v_r/c.

From Figure 4(a), one can see that the model predicts the sudden slippage of the particle, from the decelerating phase to the accelerating phase of the wakefield, which takes place when the particle is no longer highly relativistic. Again, there is an offset between the compared results in the propagated distance s at which the slippage occurs, as well as in the position ξ of the particle after the slippage. The energy loss experienced by the particle can be evaluated by

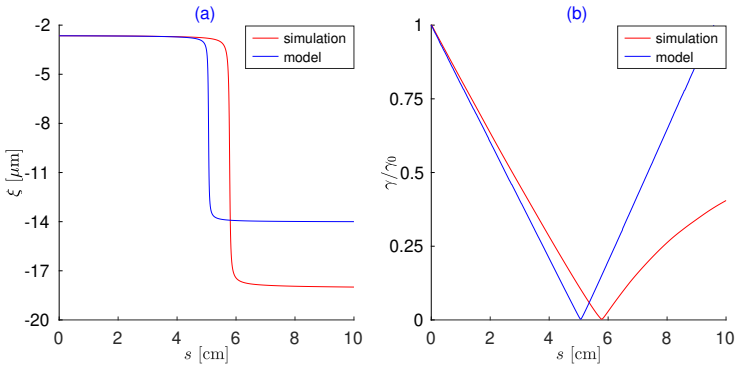

Figure 4. Longitudinal particle dynamics for (a) ξ and (b) γ/γ_0.

the evolution of its (normalised) relativistic factor γ/γ_0. This is shown in Figure 4(b) for the

simulation and model results. In both cases, this quantity exhibits the expected linear behaviour while the particle remains highly relativistic. Due to a small difference in the rates of energy loss, the particle reaches $\gamma/\gamma_0 \simeq 0$ at slightly distinct propagation distances in the model and simulation results. Since this is where the phase slippage takes place, it explains the offset in s observed in Figure 4(a). After the phase slippage, re-acceleration causes γ/γ_0 to increase. While in the simulation this growth tends to saturate, in the model γ/γ_0 increases at a constant rate.

All results presented so far show an overall good agreement between the simulation and model results. Qualitatively, the model predicts most of the behaviour observed in the PIC simulation for this particle. Quantitatively, simulation and model results differ mainly in 3 aspects: **(*i*)** changes in the particle orbit occur earlier in the model if compared to the PIC simulation, along the propagation distance s, **(*ii*)** the particle coordinate ξ after the phase slippage is smaller in the simulation than in model results, and **(*iii*)** the relativistic factor γ/γ_0 saturates in the simulation, and in the model it does not. The shift between simulation and model results described in item **(*i*)** is caused by the departure from the linear regime for the chosen parameters. The existing analytical expressions for the wakefields were derived under the assumption of small plasma density perturbations, resulting in small-amplitude fields oscillating with a sinusoidal behaviour. For a beam with peak density n_b higher than the plasma initial densisity n_0, this is not the case. As n_b/n_0 increases beyond the unit, the longitudinal wakefield E_z is sharpened, changing its shape from a sinusoidal to a sawtooth-like profile. In Figure 5(a), plotted for $r \simeq 0.04$ μm and $s \simeq 0.02$ cm, the longitudinal wakefield E_z has a steepened profile, due to $n_b/n_0 \simeq 3$. Moreover, since the amplitude of E_z in the simulation is smaller than the one given by the model, this retards all the longitudinal dynamics of simulated quantities. This explains the offset of approximately 0.4 cm along s, observed for all compared quantities plotted in the figures from this section. The difference described in the item **(*ii*)**, i.e., in the particle coordinate ξ after the phase slippage, can be also credited to the wakefield sawtooth-like profile from simulation results. As a consequence, simulation and model results have distinct values of the wakefield E_z for the same coordinate ξ. The shift shown in figure 5 is compatible with that observed after the slippage in figure 4(a). Finally, the difference of energy gain during re-acceleration, mentioned in item **(*iii*)**, is due to the self-consistent aspect of the simulations. This aspect has not yet been taken into account in the model. As decelerated beam particles suffer phase slippage, they migrate from the original beam to the re-acceleration peak, causing the wakefield amplitude to decrease. In turn, particle re-acceleration is also reduced. The self-consistent nature of this coupled process leads to saturation of energy gain in the simulation. However, in the current implementation of the semi-analytical model, the wakefield remains invariant all along the beam propagation, and no saturation is observed. Figure 5(b), plotted for $r = 0.04$ μm, at $s \simeq 10$ cm, depicts the effect of this limitation. While in the model the wakefield remains invariant, in the simulation its amplitude is drastically reduced.

6. Summary and final discussions

In this work, a short review on the advances in plasma beam dump modelling is presented. If compared to the passive case, the active scheme provides beam energy extraction with a lower (residual) chirp, over shorter propagation distances. However, the complexity and cost to implement the active case is higher than the passive one. While this might not be a problem for facilities operating laser-plasma accelerators, it may limit the adoption of the active scheme in accelerators based on beam-driven wakefields or conventional RF technology. For these cases, implementation of the passive beam dump might be the most straightforward option. For this reason, several efforts are being made to mitigate the limitations of the passive scheme. Tailored plasma-density profiles can be used to adjust the plasma wavelength along the beam, preventing the formation and growth of re-acceleration peaks by continuously defocusing the decelerated particles. Several plasma density profiles were investigated, and the obtained results

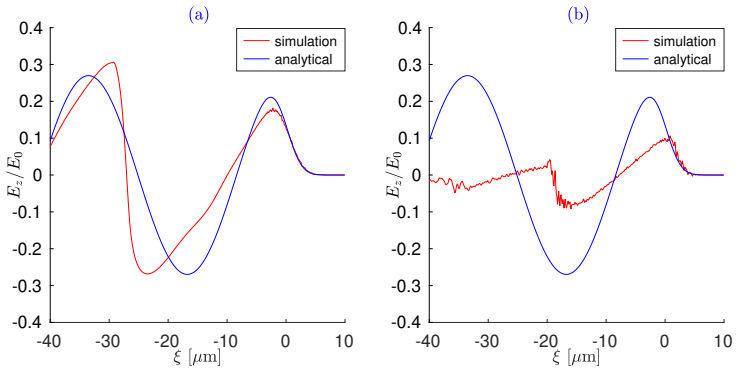

Figure 5. Comparison between the longitudinal wakefield E_z obtained with simulations and model at $r \simeq 0.04$ μm for (a) $s = 0.02$ cm, and (b) $s \simeq 10$ cm.

are encouraging. Moreover, the role of the rate of plasma wavelength change with respect to the propagation distance, $\lambda' = d\lambda/ds$, has been recently understood. In plasma-density profiles tailored to have higher values of λ', re-acceleration is mitigated by the earlier defocusing of decelerated particles, improving the overall beam energy extraction. As a last remark, the semi-analytical model under development might be a tool to better understand the wakefield-particle interaction associated with the beam deceleration process. The observed offset between simulation and model results might be reduced or even eliminated by the implementation of a self-consistent method to update the number of particles, hence the wakefield amplitude E_z, in the model. Moreover, since in this work orbits of single particles were compared, a better correspondence is expected when comparing macroscopic quantities. Due to the effect of averaging, small differences between particle orbits from simulation and model results tend to be suppressed. Finally, the implementation of the dynamics of the azimuthal coordinate θ might also improve the accuracy of the semi-analytical model.

References

[1] Tajima, T., and Dawson, J. M. (1979) Phys.Rev.Lett. 43(4), 267–270.
[2] Chen, P., Su, J. J., Dawson, J. M., Bane, K. L., and Wilson, P. B. (1986) Phys.Rev.Lett. 56(12), 1252–1255.
[3] Esarey, E., Schroeder, C., and Leemans, W. P. (2009) Rev. Mod. Phys. 81(3), 1229–1285.
[4] Gonsalves, A. *et al* . (2019) Phys. Rev. Lett. 122(8), 084801-084804.
[5] Rykovanov, S. G., *et al* . (2014) Phys. B: At., Mol. Opt. Phys. J. 47(23), 1–22.
[6] Wu, H. C., Tajima, T., Habs, D., Chao, A. W., and Meyer-ter-Vehn, J. (2010) PRSTAB 13(10), 101303.
[7] Bonatto, A., Schroeder, C. B., Vay, J. L., Geddes, C. G. R., Benedetti, C., Esarey, E., and Leemans, W. P. (2015) Phys. Plasmas 22(8), 083106–13.
[8] Chou, S., *et al* . (2016) Phys. Rev. Lett. 117(14), 144801.
[9] F. Bloch, Ann. Phys. (1933) 408, 285
[10] E. Esarey, B. A. Shadwick, P. Catravas, and W. P. Leemans (2002) Phys. Rev. E 65, 056505.
[11] Bonatto, A., Nunes, R., Xia, G. (2019) Proc. IPAC'19 3584–3586.
[12] Lehe, R., Kirchen, M., Andriyash, I. A., Godfrey, B. B., Vay, J.-L. (2016) Comput. Phys. Commun. 203, 66–82.
[13] Hanahoe, K., Xia, G., Islam, M., Li, Y., Mete-Apsimon, Ö., Hidding, B., and Smith, J. (2017) Phys. Plasmas 24(2), 023120–7.
[14] Nieter, C., and Cary, J., J. Comput. Phys. (2004) 196, 448-473.
[15] Jakobsson, O., Bonatto, A., Li, Y., Zhao, Y., Nunes, R. P., Williamson, B., Xia, G., Tajima, T. (2019) Plasma Phys. Control. Fusion 61 124002.
[16] Ariniello, R., Doss, C. E., Hunt-Stone, K., Cary, J. R., Litos, M. D. (2019) Phys. Rev. Accel. Beams 22(4), 041304.
[17] Li, X., Chancé, A., Nghiem, P. A. P. (2019) Phys. Rev. Accel. Beams 22(2), 021304.
[18] Nunes, R.P., Xia, G., Bonatto, A. (2019) Proc. IPAC'19 3581-3583.